Photothermal Response of Polyhydroxy Fullerenes

Alan Chen[†], Stephen R. Grobmyer[‡,§] and Vijay B. Krishna[*,†]

[†]Department of Biomedical Engineering, Lerner Research Institute, [‡]Surgical Oncology, Digestive Disease Institute, Cleveland Clinic, Cleveland, OH 44195

*Corresponding Author: Vijay Krishna (krishnv2@ccf.org)

[§]Current Address: *Oncology Institute, Cleveland Clinic Abu Dhabi, Abu Dhabi, United Arab Emirates*

Supplementary Figures

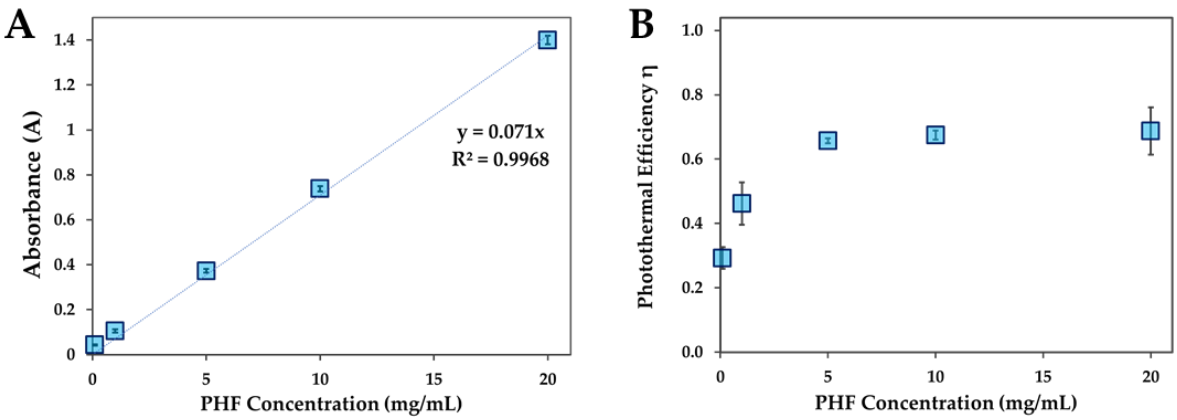

Figure S1: A) Ground state absorption of PHF as a function of concentration at 785 nm. PHF has linear absorption in tested concentrations. PHF's extinction coefficient at 785 nm is 0.071 mL/(mg cm). **B)** Photothermal conversion efficiency as a function of PHF concentration. The photothermal efficiency increases linearly at low concentrations and plateaus at higher concentrations. All experiments were conducted in triplicate (n=3) and error bars represent standard deviations.

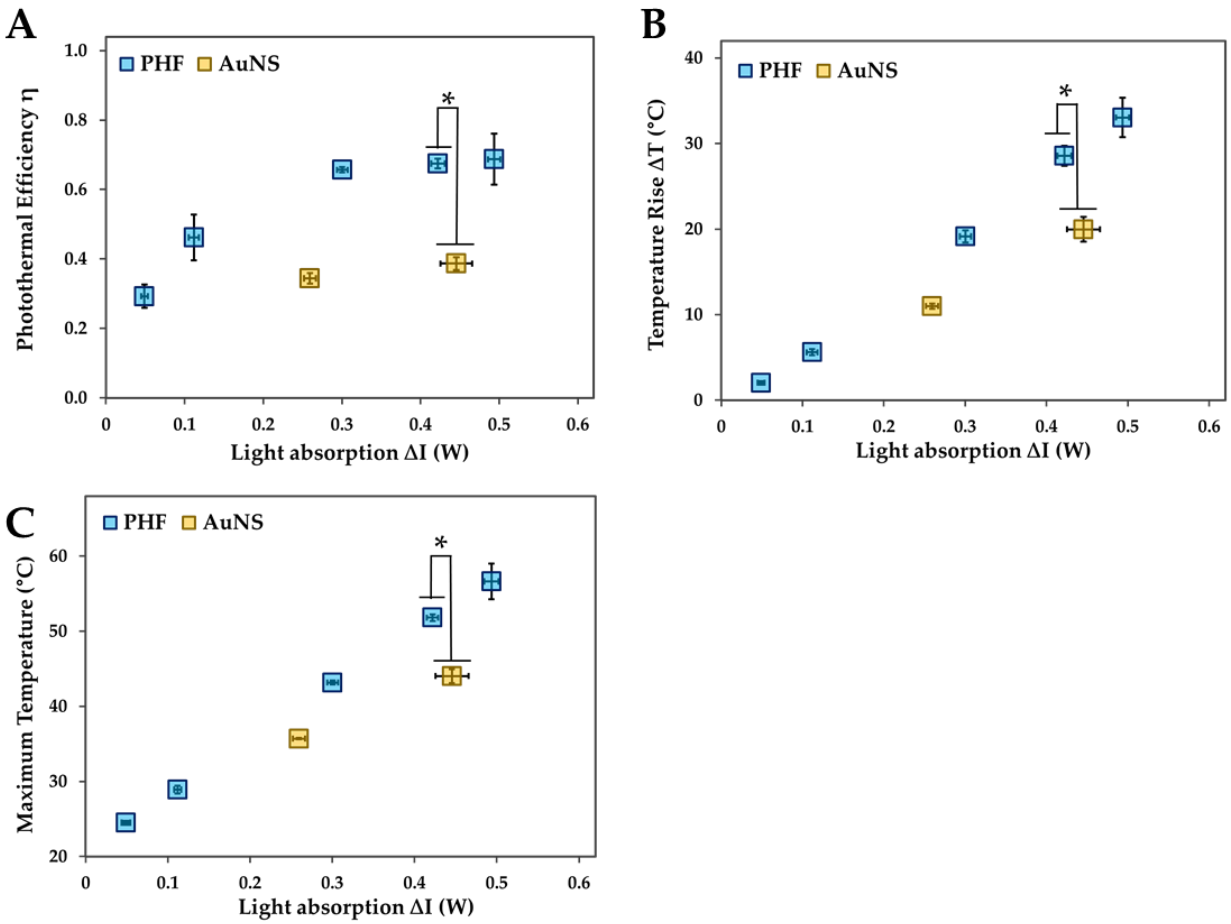

Figure S2: Effect of light absorption (***ΔI***) on **A)** photothermal efficiency (***η***), **B)** temperature rise (***ΔT***) and **C)** maximum temperature. At similar light absorptions, PHF has significantly ($p>0.01$) higher photothermal efficiency than gold nanoshells (AuNS). All experiments were conducted in triplicate (n=3) and error bars represent standard deviations. * indicates significance at α=0.01.

Table S1

Photothermal Agent	Laser Wavelength	Cuvette material	*t* (sec)	I_0 (W/cm²)	Conc of NPs	Converted Conc. (mg/mL)	η Calculation Method	η (%)	References
PHF	783 nm	PMMA	1800 (plateau)	0.5	10 mg/mL	10	optimization	69	This work
AuNS	784 nm	PMMA	1800 (plateau)	0.5	31.2 μg/mL	0.0312	optimization	39	This work
AuNS	815 nm	PMMA	2400 (plateau)	1.50	3 pM	0.0312	time constant	30	1
AuNR (8 nm)	809 nm	Quartz	1800 (plateau)	1.72	0.24 nM	0.57	time constant	95	2
AuNR (20 nm)	809 nm	Quartz	1800 (plateau)	1.72	0.24 nM	0.57	time constant	90	2
AuNR (27 nm)	980nm	Quartz	600 (plateau)	0.51	40 μg/mL	0.04	time constant	23.7	3
AuNR (30 nm)	980 nm	Quartz	360 (plateau)	1	50 μg/mL	0.05	time constant	78.8	4
AuNR (36 nm)	809 nm	Quartz	1800 (plateau)	1.72	30 μg/mL	0.03	time constant	95	5
AuNR (40 nm)	808 nm	Quartz	300 (no plateau)	0.1	*Not provided*		time constant	27-33	6
AuNR (45 nm)	815 nm	PMMA	3600 (plateau)	1.50	100 pM	0.24	time constant	55	1
AuNR (50 nm)	809 nm	Quartz	1800 (plateau)	1.72	0.24 nM	0.57	time constant	50	2
AuNR (60 nm)	809 nm	Quartz	1800 (plateau)	1.72	30 μg/mL	0.03	time constant	89	5
AuNR (60 nm)	808 nm		600 (no plateau)	0.6	25 μg/mL	0.025	time constant	39	7
AuNR (60 nm)	808 nm	PP	300 (plateau)	0.2	100 μg/mL	0.1	time constant	36.2	8
AuNR (70 nm)	809 nm	Quartz	1800 (plateau)	1.72	30 μg/mL	0.03	time constant	82	5
AuNP (5 nm)	532 nm	Quartz	1200 (plateau)	0.25	0.2 mM		time constant	80	9
AuNP (10 nm)	808 nm	Quartz	300 (no plateau)	0.1	*Not provided*		time constant	9	6

AuNP (15 nm)	532 nm	Quartz	1200 (plateau)	0.25	0.2 mM		time constant	78	9
AuNP (20 nm)	514 nm	Quartz	320 (plateau)	0.17	920 μg/mL	0.92	time constant	8	10
AuNP (50 nm)	532 nm	Quartz	1200 (plateau)	0.25	0.2 mM		time constant	65	9
AuNP (127 nm)	809 nm	Quartz	1800 (plateau)	1.72	33 μg/mL	0.033	time constant	60	5
AuNP (l54 nm)	809 nm	Quartz	1800 (plateau)	1.72	33 μg/mL	0.033	time constant	45	5
Au Nano Cube (10 nm)	808 nm	Quartz	300 (no plateau)	0.1	*Not provided*		time constant	15	6
AuNR-CuS (60 nm)	808 nm		600 (no plateau)	0.6	25 μg/mL	0.025	time constant	62	7
AuNP-Co (50 nm)	790 nm		1800 (plateau)	1.0	0.2 mg/mL	0.2	time constant	99	11
Au/Mo-ICG (110 nm)	808 nm	PP	300 (plateau)	0.2	100 μg/mL	0.1	time constant	68.8	8
Au-Pt Nanoraspberries	650 nm	Quartz	300 (no plateau)	0.1	*Not provided*		time constant	61	12
Au-Pt Nanoraspberries	808 nm	Quartz	300 (no plateau)	0.1	*Not provided*		time constant	52	12
AgI-AgS2 Nanostructure	808 nm	Quartz	3000 (no plateau)	0.42	0.01% wt	10	time constant	33.4	13
NiS2, Mesoporous	808 nm	Quartz	600 (no plateau)	2	20 μg/mL	0.02	time constant	44.6	14
Liquid Metal NR	808 nm	PS	250 (no plateau)	3.5	800 mg/L	0.8	time constant	25.3	15
GaNS	808 nm	PS	250 (no plateau)	3.5	800 mg/L	0.8	time constant	25.3	15
GaNR	808 nm	PS	250 (no plateau)	3.5	800 mg/L	0.8	time constant	32.7	15
Cu Nanocluster	980 nm	Quartz	600 (plateau)	0.51	40 μg/mL	0.04	time constant	25.7	3
Cu Nanocluster	800 nm	Quartz	300 (no plateau)	2	1 mg/mL	1	time constant	22	16

Pt Nanoparticles (2 nm)	808 nm	Quartz	300 (no plateau)	0.1			time constant	33	17
Pt Nanoparticles (80 nm)	808 nm	Quartz	300 (no plateau)	0.1			time constant	15	17
ICG	808 nm	PS	180 (no plateau)	1.1	5 μg/mL	0.005	time constant	3.37	18
Cyanine Micelles	808 nm		600 (no plateau)	0.7	5 ug/mL	0.005		47	19
Organic Drug	635 nm		300 (no plateau)	0.5	0.5 mM		time constant	37	20
Carbon Nanospheres	808 nm	PS	600 (no plateau)	1.5	100 μg/mL	0.1	time constant	35.7	21

t = Laser irradiation time; I_0 = Incident laser power; η = Photothermal conversion efficiency

References

1. Cole, J. R.; Mirin, N. A.; Knight, M. W.; Goodrich, G. P.; Halas, N. J., Photothermal Efficiencies of Nanoshells and Nanorods for Clinical Therapeutic Applications. *J. Phys. Chem. C* **2009,** *113* (28), 12090-12094.
2. Chen, H.; Shao, L.; Ming, T.; Sun, Z.; Zhao, C.; Yang, B.; Wang, J., Understanding the photothermal conversion efficiency of gold nanocrystals. *Small* **2010,** *6* (20), 2272-80.
3. Tian, Q.; Jiang, F.; Zou, R.; Liu, Q.; Chen, Z.; Zhu, M.; Yang, S.; Wang, J.; Wang, J.; Hu, J., Hydrophilic Cu9S5 Nanocrystals: A Photothermal Agent with a 25.7% Heat Conversion Efficiency for Photothermal Ablation of Cancer Cells in Vivo. *ACS Nano* **2011,** *5* (12), 9761-9771.
4. Bi, C.; Chen, J.; Chen, Y.; Song, Y.; Li, A.; Li, S.; Mao, Z.; Gao, C.; Wang, D.; Möhwald, H.; Xia, H., Realizing a Record Photothermal Conversion Efficiency of Spiky Gold Nanoparticles in the Second Near-Infrared Window by Structure-Based Rational Design. *Chem. Mater.* **2018,** *30* (8), 2709-2718.
5. Jiang, K.; Smith, D. A.; Pinchuk, A., Size-Dependent Photothermal Conversion Efficiencies of Plasmonically Heated Gold Nanoparticles. *J. Phys. Chem. C* **2013,** *117* (51), 27073-27080.
6. Depciuch, J.; Stec, M.; Kandler, M.; Baran, J.; Parlinska-Wojtan, M., From spherical to bone-shaped gold nanoparticles-Time factor in the formation of Au NPs, their optical and photothermal properties. *Photodiagn. Photodyn. Ther.* **2020**, 101670.
7. Leng, C.; Zhang, X.; Xu, F.; Yuan, Y.; Pei, H.; Sun, Z.; Li, L.; Bao, Z., Engineering Gold Nanorod-Copper Sulfide Heterostructures with Enhanced Photothermal Conversion Efficiency and Photostability. *Small* **2018,** *14* (12), e1703077.
8. Younis, M. R.; Wang, C.; An, R.; Wang, S.; Younis, M. A.; Li, Z.-Q.; Wang, Y.; Ihsan, A.; Ye, D.; Xia, X.-H., Low Power Single Laser Activated Synergistic Cancer Phototherapy Using Photosensitizer Functionalized Dual Plasmonic Photothermal Nanoagents. *ACS Nano* **2019,** *13* (2), 2544-2557.
9. Jiang, R.; Cheng, S.; Shao, L.; Ruan, Q.; Wang, J., Mass-Based Photothermal Comparison Among Gold Nanocrystals, PbS Nanocrystals, Organic Dyes, and Carbon Black. *J. Phys. Chem. C* **2013,** *117* (17), 8909-8915.
10. Roper, D. K.; Ahn, W.; Hoepfner, M., Microscale Heat Transfer Transduced by Surface Plasmon Resonant Gold Nanoparticles. *J. Phys. Chem. C* **2007,** *111* (9), 3636-3641.
11. Lindley, S. A.; Zhang, J. Z., Bumpy Hollow Gold Nanospheres for Theranostic Applications: Effect of Surface Morphology on Photothermal Conversion Efficiency. *ACS Appl. Nano Mater.* **2019,** *2* (2), 1072-1081.
12. Depciuch, J.; Stec, M.; Klebowski, B.; Baran, J.; Parlinska-Wojtan, M., Platinum-gold nanoraspberries as effective photosensitizer in anticancer photothermal therapy. *J. Nanobiotechnol.* **2019,** *17* (1), 107.
13. Zeng, W.; Suo, L.; Zhang, C.; Wu, D.; Zhu, H., AgI–Ag2S heterostructures for photothermal conversion and solar energy harvesting. *J. Taiwan Inst. Chem. Eng.* **2019,** *95*, 273-280.

14. He, G.; Ma, Y.; Zhou, H.; Sun, S.; Wang, X.; Qian, H.; Xu, Y.; Miao, Z.; Zha, Z., Mesoporous NiS2 nanospheres as a hydrophobic anticancer drug delivery vehicle for synergistic photothermal–chemotherapy. *J. Mater. Chem. B* **2019,** *7* (1), 143-149.
15. Sun, X.; Sun, M.; Liu, M.; Yuan, B.; Gao, W.; Rao, W.; Liu, J., Shape tunable gallium nanorods mediated tumor enhanced ablation through near-infrared photothermal therapy. *Nanoscale* **2019,** *11* (6), 2655-2667.
16. Hessel, C. M.; Pattani, V. P.; Rasch, M.; Panthani, M. G.; Koo, B.; Tunnell, J. W.; Korgel, B. A., Copper Selenide Nanocrystals for Photothermal Therapy. *Nano Lett.* **2011,** *11* (6), 2560-2566.
17. Depciuch, J.; Stec, M.; Klebowski, B.; Maximenko, A.; Drzymala, E.; Baran, J.; Parlinska-Wojtan, M., Size effect of platinum nanoparticles in simulated anticancer photothermal therapy. *Photodiagn. Photodyn. Ther.* **2020,** *29*, 101594.
18. Yoon, H.-J.; Lee, H.-S.; Lim, J.-Y.; Park, J.-H., Liposomal Indocyanine Green for Enhanced Photothermal Therapy. *ACS Appl. Mater. Interfaces* **2017,** *9* (7), 5683-5691.
19. Li, L.; Yang, Q.; Shi, L.; Zheng, N.; Li, Z.; Li, K.; Qiao, S.; Jia, T.; Sun, T.; Wang, Y., Novel phthalocyanine-based polymeric micelles with high near-infrared photothermal conversion efficiency under 808 nm laser irradiation for in vivo cancer therapy. *J. Mater. Chem. B* **2019,** *7* (14), 2247-2251.
20. Wang, H.; Chang, J.; Shi, M.; Pan, W.; Li, N.; Tang, B., A Dual-Targeted Organic Photothermal Agent for Enhanced Photothermal Therapy. *Angew. Chem., Int. Ed. Engl.* **2019,** *58* (4), 1057-1061.
21. Weng, Y.; Guan, S.; Wang, L.; Qu, X.; Zhou, S., Hollow carbon nanospheres derived from biomass by-product okara for imaging-guided photothermal therapy of cancers. *J. Mater. Chem. B* **2019,** *7* (11), 1920-1925.